Exploration Geophysics

ISSN: 0812-3985 (Print) 1834-7533 (Online) Journal homepage: https://www.tandfonline.com/loi/texg20

# Mapping pollution and coastal hydrogeology with helicopterborne transient electromagnetic measurements

Niels B. Christensen & Max Halkjær

**To cite this article:** Niels B. Christensen & Max Halkjær (2014) Mapping pollution and coastal hydrogeology with helicopterborne transient electromagnetic measurements, Exploration Geophysics, 45:4, 243-254, DOI: 10.1071/EG13071

**To link to this article:** https://doi.org/10.1071/EG13071

Published online: 07 Dec 2018.

CSIRO PUBLISHING

*Exploration Geophysics*, 2014, **45**, 243–254
http://dx.doi.org/10.1071/EG13071

# Mapping pollution and coastal hydrogeology with helicopterborne transient electromagnetic measurements

Niels B. Christensen[1,3] Max Halkjær[2]

[1]Department of Geoscience, Aarhus University, C F Moellers Allé 4, DK-8000 Aarhus C, Denmark.
[2]Rambøll A/S, Hannemanns Allé 53, 2300 København S, Denmark.
[3]Corresponding author. Email: nbc@geo.au.dk

**Abstract.** Coastal hydrology is becoming the focus of increasing interest for several reasons. Hydrogeological models need good boundary conditions at the coastline, and with the expected sea level rise due to climate changes, it becomes increasingly important to grasp the dynamics of coastal hydrology in order to predict the consequences of sea level rise for nature and society.

We present a helicopterborne transient electromagnetic survey from a region at the North Sea coast in western Jutland, Denmark, carried out at a seriously polluted site with the dual purpose of assessing the extent of the pollution and mapping the coastal hydrogeology to provide data for remediation activities. Data are subjected to constrained inversion with one-dimensional multi-layer (smooth) models. The extent of the pollution plume estimated from a conductive anomaly in the survey results is mainly in accordance with results from other investigations, but also points to hitherto unknown directions of seepage. The interleaving of freshwater extending under the offshore shallow sea and saltwater infiltrating under the onshore freshwater aquifer can be clearly discerned and preferential flow channels are revealed.

Received 18 August 2013, accepted 28 January 2014, published online 17 March 2014

## Introduction

The hydrogeology of coastal regions is an important field of study that any country will have to consider. Often major cities with their concentrated populations are situated at the coast and the challenge of making sufficient amounts of good quality water available to large urban populations is complicated by saltwater intrusion in aquifers, pollution from large volumes of sewage, waste and the industrial pollution produced by that same population. It is a difficult balancing act between conflicting interests to build and maintain a water infrastructure that will ensure that the basic needs of large population concentrations are met (United Nations, 2006). At the same time, coastal regions are often important for recreational activities where the quality and safety of the environment is important. The expected sea level rise and more frequent extreme weather conditions due to climate changes emphasise the importance of understanding the dynamics of coastal hydrology (United Nations, 2004; Beuhler, 2003).

Transient electromagnetic (TEM) soundings have become one of the standard methods of environmental geophysics with a wide variety of applications (Fitterman and Stewart, 1986; Auken et al., 2006; Christensen, 2009; Steuer et al., 2009). TEM measurements delineate good conductors well, such as clay and saltwater, thereby assisting hydrogeological modelling efforts by providing information on important formation boundaries and formation characteristics. Over the past two decades, airborne TEM methods have found widespread use in hydrogeophysical investigations, making it possible to cover large areas in a cost-effective way.

Airborne EM methods have been increasingly used in connection with mapping of pollution, the target being the conductive anomalies associated with high acid, base or salt contents of the polluting substance itself or associated with the chemical production and use of organic compounds. In areas difficult to access using surface methods, including dams with permanent water cover or those located in rugged terrain, airborne methods providing continuous coverage can be a cost-effective adjunct to drilling or small-scale surface surveys, and are used to more effectively target surface investigations.

Examples of mapping of mine tailings or waste materials from coal power generation and metals refining are given in Rutley and Fallon (2000), Morris et al. (2002), Hammack et al. (2005) and Beamish and Klinck (2006). The surveys reported by these authors used helicopterborne frequency-domain systems. The use of airborne time domain methods to map dump sites has been reported by Silvestri et al. (2009), and in Reid et al. (2012), a fly ash deposit and its possible pollution plume were mapped.

Due to the effect of gravity on the specific mass difference between saltwater and freshwater, saltwater infiltrates below the fresh groundwater in the near-coastal zone (Sulzbacher et al., 2011). The presence of the saltwater can affect the availability of freshwater at considerable distances from the coastline (Shtivelman and Goldman, 2000). The extent of the affected zone depends critically on the distribution of hydraulic conductivity (lithology) and the hydraulic gradient, and may stretch several hundreds of metres inland from the coast in the Danish environment. The problem is aggravated if freshwater is abstracted in the coastal zone to the extent that the hydraulic gradient begins to point landward which often happens around major coastal cities. The phenomenon is also serious for small islands where the available freshwater is often limited to a rather thin lens floating on the deep saltwater intrusion.

There are several examples of airborne EM methods being used to map the coastal zone. A large survey with both frequency

 

and time domain helicopterborne systems and ground EM measurements was carried out in the Everglades National Park, Florida, USA (Fitterman and Deszcz-Pan, 1998; Fitterman et al., 1999) to map the distribution of saltwater and freshwater. Quite a few studies have been carried out in north-western Europe (Faneca Sànchez et al., 2012; Steuer et al., 2009); in particular, the island of Borkum in Germany has been investigated extensively (Wiederhold et al., 2013; Sulzbacher et al., 2011, 2012; Günther and Müller-Petke, 2012). Other studies (Kirkegaard et al., 2011) have demonstrated that the use of airborne EM methods can achieve the goal of obtaining a three-dimensional water quality model to be used in groundwater modelling.

The Bandah Aceh survey conducted after the Boxing Day 2004 tsunami by Siemon et al. (2007) is a rather unique application of airborne EM measurements to map saltwater intrusion and saltwater flooding in aquifers. With the helicopterborne frequency domain system of BGR (Bundesanstalt für Geowissenschaften und Rohstoffe: Federal Institute for Geosciences and Natural Resources, Hannover, Germany), a comprehensive survey was conducted to map pockets of freshwater unaffected by the saltwater flood caused by the tsunami.

Less investigated is the fact that freshwater infiltrates through subbottom sediments under the ocean to considerable distances from the shore line. Partly driven by the differential gravity effect of freshwater and saltwater, and partly by the hydraulic head and the distribution of fine and coarse sediments, the pattern of the freshwater infiltration can be quite complicated, and it is not straightforward to estimate either the total flux of freshwater along the coast or its degree of inhomogeneity (Langevin, 2003; Viezzoli et al., 2010; Teatini et al., 2011). This gives rise to uncertain boundary conditions in hydrogeological models of coastal areas. Part of the reason for the lack of knowledge is the difficulty in mapping the small differences in conductivity between freshwater and saltwater and the zone of mingling in

**Table 1. Estimated mass of pollutants at Kærgaard Plantation.**
NVOC: non-volatile organic carbon

| Chemical compound | Estimated mass (t) |
|---|---|
| Chlorinated solvents | 340 |
| Hydrocarbons | 225 |
| Sulfonamides | 230 |
| NVOC | 1600 |

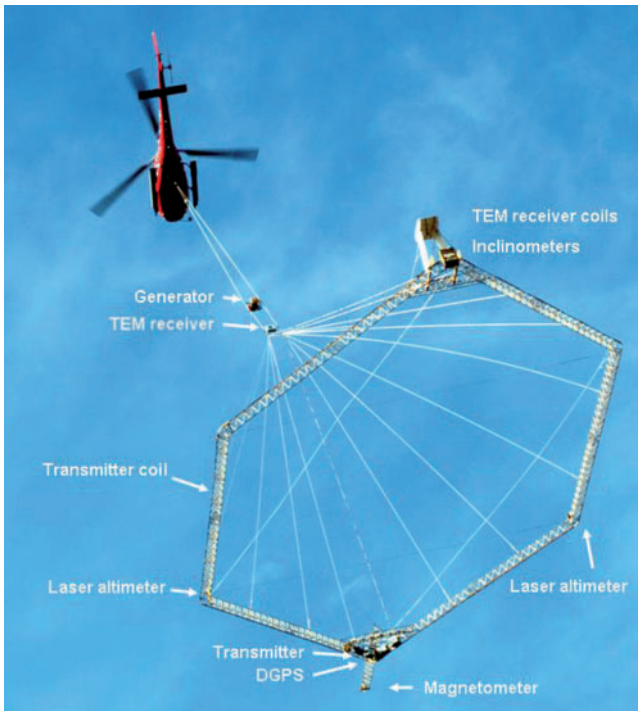


**Fig. 1.** The SkyTEM system at a glance.

**Table 2. SkyTEM survey parameters for the super-low moment (SLM) and the high moment (HM).**

| Survey parameter | SLM | HM |
|---|---|---|
| Tx area ($m^2$) | 494.4 | 494.4 |
| Tx moment ($Am^2$) | 5240 | 184 000 |
| Nominal Tx height (m) | 30 | 30 |
| Repetition frequency (Hz) | 250 | 25 |
| Nominal ground speed (km/h) | 45 | 45 |
| First gate (μs) | 10.5 | 141 |
| Last gate (ms) | 0.714 | 8.84 |
| Number of gates | 21 | 19 |
| Rx cutoff frequency (kHz) | 450 | 450 |
| Amplifier cutoff frequency (kHz) | 300 | 300 |
| Front gate (μs) | N/A | 69.5 |

**Fig. 2.** Location map of Kærgaard, Denmark.

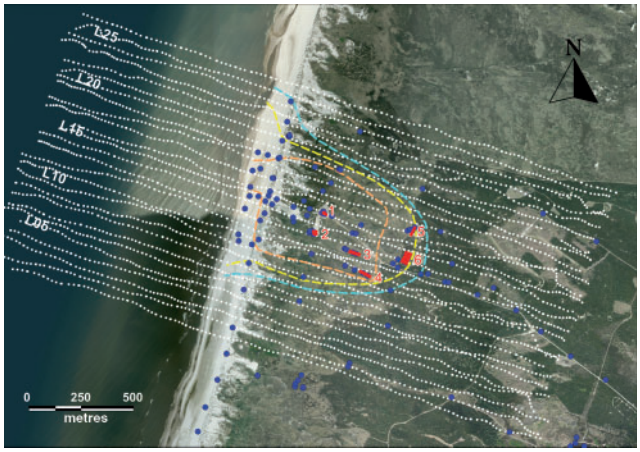


**Fig. 3.** The survey area. Flight lines indicated with white dots and line numbers for every five lines; pits indicated with red rectangles and selected bores with small blue circles. The blue, yellow and orange broken lines are isolines for the pore water conductivity determined from water samples from the bores for the values 50, 100 and 1000 mS/m, respectively.

coastal areas, but with modern, well calibrated and stable helicopterborne TEM systems, such mapping can now be undertaken.

In this paper, we will demonstrate the potential of an airborne TEM survey to assist in mapping the extent of pollution at a North Sea coastal site in Denmark and the distribution of

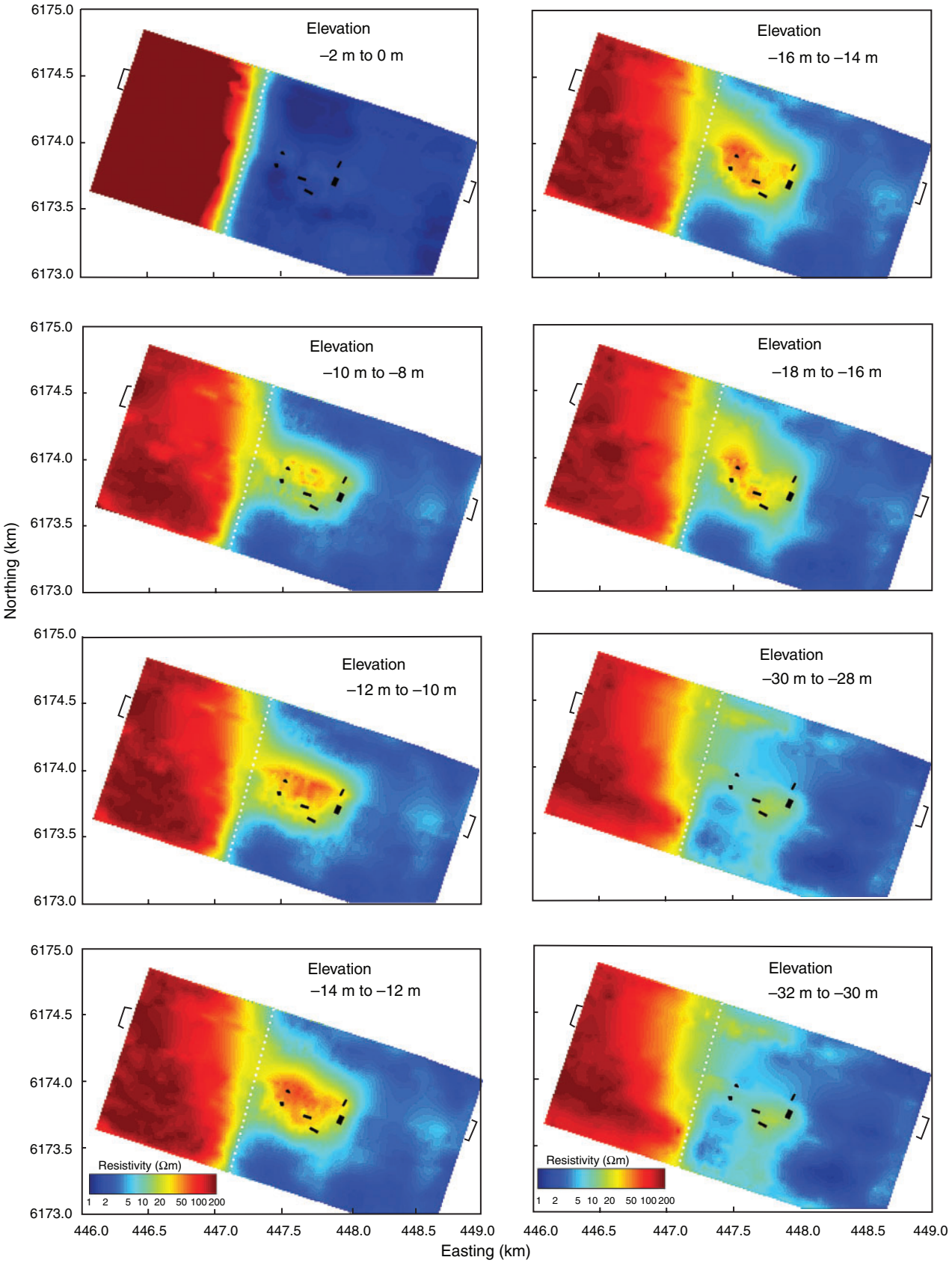


**Fig. 4.** Mean resistivity in elevation intervals. The white dots indicate the coastline. The black rectangles indicate the dumping pits. The black brackets indicate the positions of the discarded Lines 17–20.

freshwater and saltwater in the coastal zone. Data are inverted with one-dimensional multi-layer (smooth) models employing a least-squares iterative constrained inversion procedure. We present the results as model sections and as maps of mean conductivity in elevation intervals. The extent of the pollution plume is clearly indicated in the survey results, and a complex pattern of interleaving freshwater and saltwater at the coastline can be discerned from the interpreted sections.

## Inversion methodology

### *Damped least-squares inversion*

In this study, we shall use the well-established iterative damped least squares approach to the inversion of EM data with a 1D model consisting of horizontal, homogeneous and isotropic layers. Formally, the model update at the *n*th iteration is given by (Menke, 1989)

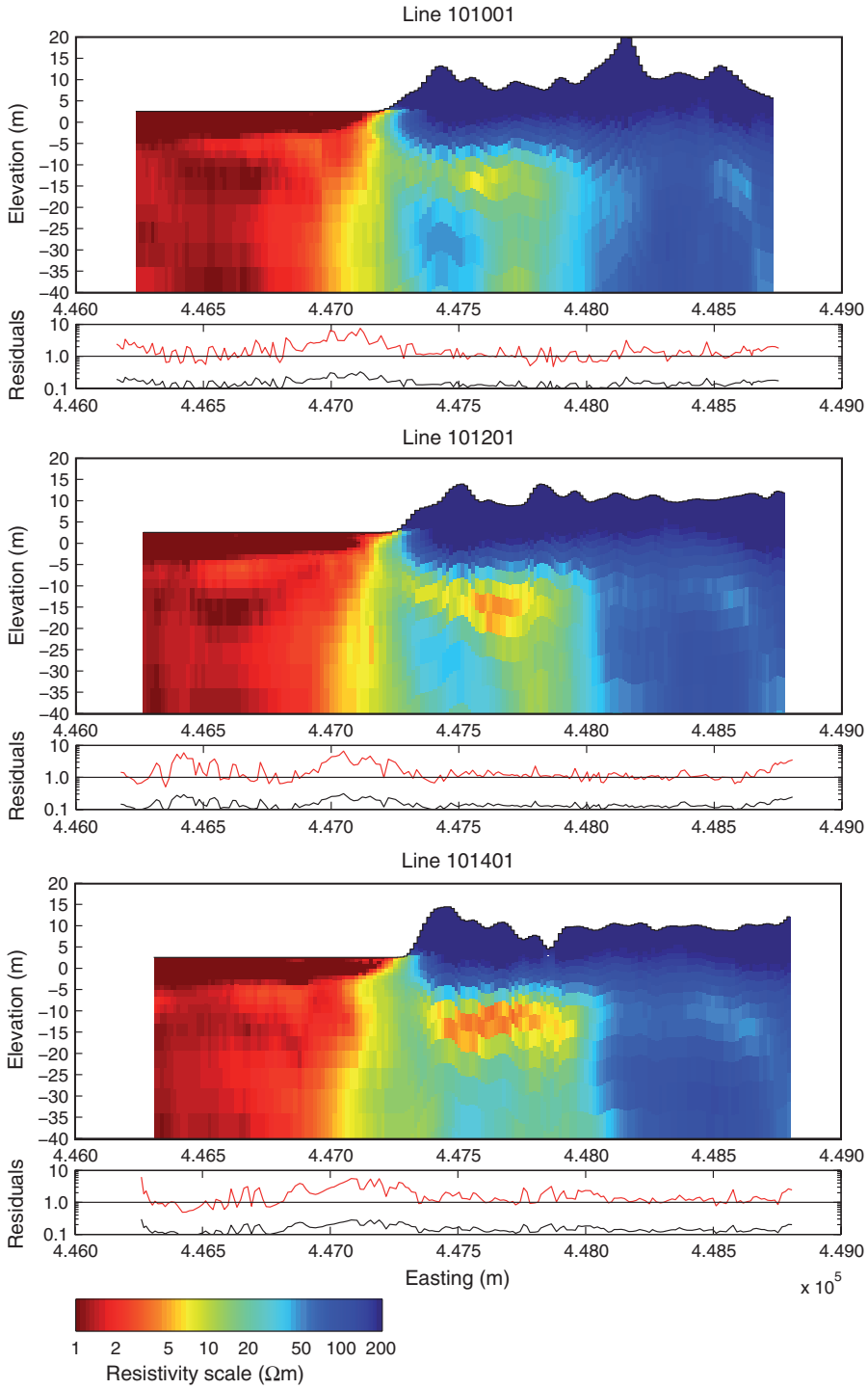


**Fig. 5.** Model sections of Lines 10, 12, 14 and 16 to a depth of 40 m. The data residual (red) and total residual (black) of the inversion is plotted below the model section. The elevation of the sea surface reflects the coordinate projection used (UTM WGS84 Z32) and the tidal situation on the day of data acquisition.

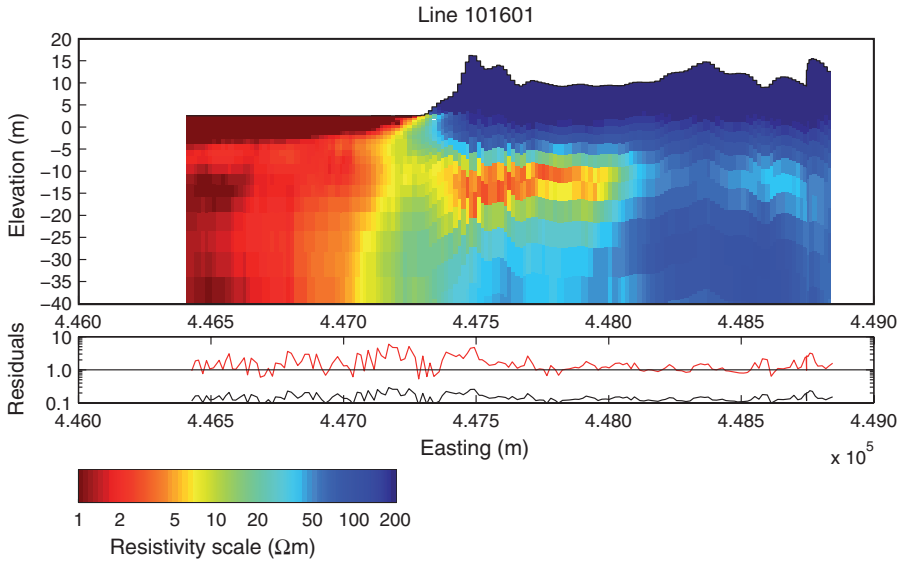


**Fig. 5.** (*continued*)

$$\boldsymbol{m}_{n+1} = \boldsymbol{m}_n + \left[\boldsymbol{G}_n^T\, \boldsymbol{C}_{obs}^{-1}\boldsymbol{G}_n + \boldsymbol{C}_m^{-1}\right]^{-1} \cdot \left[\boldsymbol{G}_n^T\boldsymbol{C}_{obs}^{-1}(\boldsymbol{d}_{obs} - \boldsymbol{g}(\boldsymbol{m}_n)) + \boldsymbol{C}_m^{-1}\left(\boldsymbol{m}_{prior} - \boldsymbol{m}_n\right)\right] \quad (1)$$

where $\boldsymbol{m}$ is the model vector containing the logarithm of the model parameters, $\boldsymbol{G}$ is the Jacobian matrix containing the derivatives of the data with respect to the model parameters, $T$ is the matrix transpose, $\boldsymbol{C}_{obs}$ is the data error covariance matrix, $\boldsymbol{C}_m$ is a model covariance matrix imposing the vertical smoothness constraint of the multi-layer models, $\boldsymbol{d}_{obs}$ is the field data vector, $\boldsymbol{g}(\boldsymbol{m}_n)$ is the nonlinear forward response vector of the $n$th model, and $\boldsymbol{m}_{prior}$ is the prior model vector. In this study, as is most often the case, the data noise is assumed to be uncorrelated, implying that $\boldsymbol{C}_{obs}$ is a diagonal matrix.

The model parameter uncertainty estimate relies on a linear approximation to the posterior covariance matrix, $\boldsymbol{C}_{est}$, given by

$$\boldsymbol{C}_{est} = \left[\boldsymbol{G}^T\boldsymbol{C}_{obs}^{-1}\boldsymbol{G} + \boldsymbol{C}_m^{-1}\right]^{-1} \quad (2)$$

where $\boldsymbol{G}$ is based on the model achieved after the last iteration. The analysis is expressed through the standard deviations of the model parameters obtained as the square root of the diagonal elements of $\boldsymbol{C}_{est}$ (e.g. Inman et al., 1975).

### *1D models*

Inversion is carried out using multi-layer models, sometimes called 'smooth' models, that divide the subsurface into a large number of layers. In the iterative inversion, the layer boundaries are kept fixed and only the layer conductivities are updated. In this study, we have used a 30-layer model with a top layer thickness of 0.5 m and a depth to the bottom layer boundary of 200 m. The depths to the layer boundaries increase downwards as a hyperbolic sine of the layer number. In this way, the depths to the layer boundaries increase linearly for small depths so that the top layers are all of approximately the same thickness, and the depths to the layer boundaries increase exponentially at large depths so that the thickness of a layer is a factor times the previous one; for this model, a factor of 1.18, corresponding to 13.6 layers per decade.

### *Vertical model constraints*

To avoid geologically irrelevant models, constraints on the vertical variability of model conductivity are imposed through the use of a model covariance matrix, $\boldsymbol{C}_m^{-1}$ in equation 1. The covariance matrix is based on an approximation to a von Karman covariance function given by

$$\Phi_{\nu, L_N} \approx \sigma_0^2 \sum_{n=0}^{N} C^{n\cdot\nu} \exp\left(\frac{-|z|}{C^n L_N \cdot 0.65}\right) \quad (3)$$

where $L_N$ is the maximum correlation length represented, $C$ is the factor ($C<1$) between the correlation lengths, $N$ is the number of stacked single-scale covariance functions and $\sigma_0$ is the standard deviation of the correlation. The factor 0.65 in the exponential denominator is an empirical factor that improves the fit to the von Karman function. The resulting stacked covariance function is essentially free of correlation scale. The lower and upper limits of the correlation lengths are a mathematical convenience and do not influence the correlation properties at the distance scales typically studied (Serban and Jacobsen, 2001; Christensen et al., 2009*a*). This broadband behaviour ensures superior robustness in the inversion, i.e., model structure on all scales will be permitted if required by the data, and it makes the regularisation imposed by the model covariance matrix insensitive to the discretisation (Serban and Jacobsen, 2001).

In this study, we have used $\nu = 0.1$, $C = 0.1$, $L_N = 10\,000$ km and $N = 10$. This means that the covariance function will contain correlation lengths between 6500 km and 6.5 mm, one per decade. This covers scales of geological variability between the radius of the Earth and pebbles, clearly sufficient for the resolution capability of airborne TEM data. The model covariance matrix only depends on the geometry of the multi-layer model and so it needs to be calculated and inverted only once.

It is crucial for a successful inversion with multi-layer models to choose the correlation standard deviation, $\sigma_0$, correctly in relation to the information content of the data. If $\sigma_0$ is too small, the model will not show all the structures that can be resolved by the data, and if $\sigma_0$ is too large, the models will become erratic and the inversion will fit the data noise. The practical inversion is done on the logarithm of resistivities and the model covariance matrix thus relates to this parameter. We have chosen the strength of the regularisation to be $\sigma_0 = 2.0$ through a pragmatic process of visually inspecting the results of using several different regularisation levels.

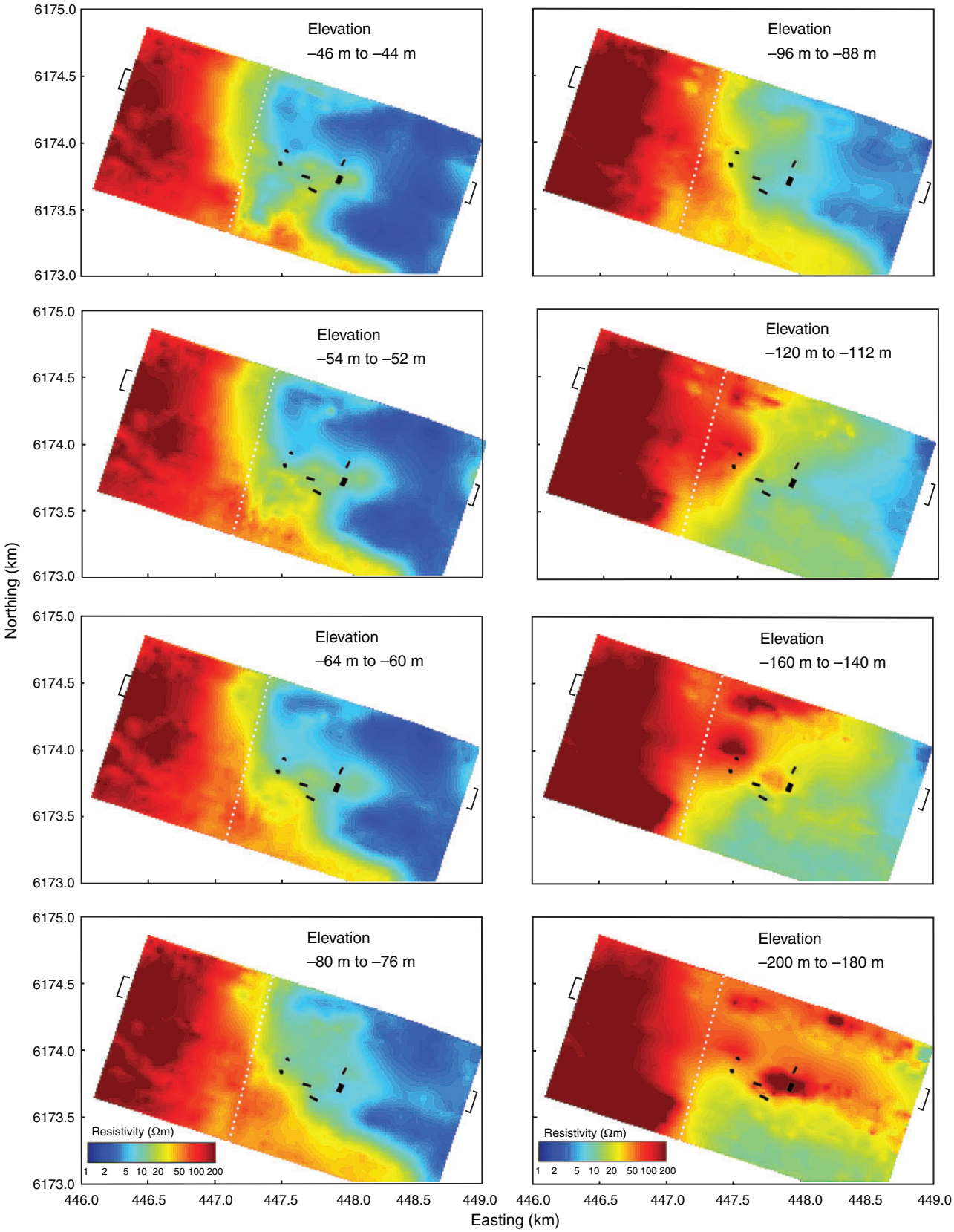


**Fig. 6.** Mean resistivity in elevation intervals. The white dots indicate the coastline. The black brackets indicate the positions of the discarded Lines 17–20.

*Model inconsistency, coupling and lateral correlation*

1D inversion is justified where lateral changes in conductivity are gradual. In this case, the pseudo-2D images produced by concatenating 1D models along the profile will give a good approximation to the real conductivity distribution. The effects of 3D structures on 1D interpretation of TEM data have been dealt with in a number of papers, e.g. Newman et al. (1987), Goldman et al. (1994), and Hördt and Scholl (2004). In general,

these studies show that, if the geological environment consists of slowly varying 3D structures with moderate conductivity contrasts, the 1D inversion approach is viable, even though a successful inversion that finds a model fitting the data is not sufficient to conclude that 3D effects are absent (Ellis, 1998). In environments with pronounced 3D model characteristics, 1D inversion is strongly influenced by 3D effects and will in many cases provide unreliable models with artifacts known as 'pant legs'. Such effects can be seen at the coastline where the very conductive body of seawater terminates.

Another type of 3D effect, namely coupling between the AEM system and man-made good conductors, was found where a gas pipeline and an oil pipeline traverse the northern part of the survey area, almost coincident with Line 19. In this case we have coupling between the steel pipelines and the transmitted EM field. The coupling affects Lines 17–20 and these were removed from the survey before inversion so that they would not affect the final results.

In most parts of the survey area, lateral changes are small, but because of the local character of the data noise in space and time, individual inversion of the sounding data does not ensure lateral continuity of the model sections and it is therefore reasonable to impose continuity by lateral correlation of the models. Techniques for lateral correlation of 1D earth models have been presented by, e.g., Gyulai and Ormos (1999) and Auken and Christiansen (2004) (Auken et al., 2005). In this paper, we apply the lateral parameter correlation (LPC) procedure of Christensen and Tølbøll (2009). We have chosen to use the same broadband covariance matrix for the lateral correlation as for the vertical smoothness. Using the broadband covariance matrix is equivalent to an assumption that the variability of the geology is fractal, and using the same for vertical and horizontal regularisation means that we have no assumptions that the vertical and horizontal variability are different. Using the same pragmatic approach, we have chosen $\sigma_0 = 0.4$, pertaining to log (resistivity), in the lateral correlation. We have deliberately chosen the lateral correlation to be quite weak. In this way, we obtain smoothness in the areas where it is justified, and we avoid smoothing the model section so much that we cannot identify 3D and coupling effects where they might appear. The LPC method is inherently multidimensional and the procedure was carried out in the plane on all soundings on all profile lines simultaneously.

## Kærgaard Plantation

### *A coastal polluted site*

Kærgaard Klitplantage (Kærgaard Dune Plantation) is situated at the west coast of southern Jutland, Denmark, towards the North Sea. It is one of the most seriously polluted sites in Denmark, with major ongoing remediation activities over the past decades. Until the extent of the pollution was realised, the area was used as military training grounds, a nature reserve and recreational area with tourism and holiday activities, mainly in the summer time. From 1956 until 1973, untreated wastewater from a chemical plant was dumped into six pits in the plantation 400–800 m from the coastline. The waste contained a mixture of chlorinated organic solvents, hydrocarbons, sulfonamides and other substances and the estimated mass of pollutants is listed in Table 1 (Miljøstyrelsen, 2005). The risk assessment lists the following main problems: breathing of volatile components around the pits and at the beach; offensive smell; contact with polluted sand at the beach; contact with polluted water at the beach and in the sea; and evidently flora and fauna are affected by the pollution. The pollution is known to move seawards and 3 km of the beach is now closed to the public.

Remediation efforts began sporadically in the 1980s, but dedicated efforts were not initiated until around 2004. So far, remediation efforts have cost €7 million and further efforts are budgeted to €60 million. It is, however, anticipated that the total cost of remediation could go as high as €90 million.

### *Geology, hydrogeology and bathymetry of the area*

The survey area is characterised by postglacial sediments. It was created as a barrier coast with inlet and tidal canal systems, and a complex geological setting was built up through alternate layers of coarse-grained permeable sediments deposited during periods of high energy density, and silty and clayey material deposited in the same canals in periods where they were closed off to the ocean. Seaward from the present coastline, fine-grained marine sediments dominate (Ribe Amtskommune, Miljoministeriet, Danmarks Geologiske undersogelse, Skov- og Naturstyrelsen, 1989; Arbejdsgruppen vedrørende Kærgård Plantage, 2006)

In the polluted area, ~180 boreholes have been drilled and measurements of groundwater conductivity been made, but none of them were drilled to a depth exceeding 20–25 m in order not to penetrate a rather impermeable silt layer at that depth and thereby spread the pollution to deeper layers. Above the silty layer, the geology is dominated by high permeability sand.

The deeper geology is poorly known which is quite unusual in a country as densely populated as Denmark, but the location is rather isolated with little farming, industry or major settlements and no deep boreholes have been drilled, e.g. for water. It is not known at which depth Tertiary sediments will be found, but, regionally, Miocene sandy and silty formations are found in the upper Tertiary and at greater depths heavy Paleocene clays are known to exist. This state of affairs makes it challenging to discern whether high conductivity formations are saltwater infiltrated sediments or clayey formations.

The bathymetry is characterised by a slow, almost linear, increase in water depth of 10 m per kilometre from the coast and seawards with small, local decreases in water depth at the three sand bars that exist in the area. The seawater conductivity at the North Sea coast is around 4 S/m.

### *The airborne TEM survey*

The airborne TEM survey was carried out with the SkyTEM system (see Figure 1), a helicopterborne TEM system (Sørensen and Auken, 2004) originally designed and developed for hydrogeophysical and environmental investigations. The aim was to develop an airborne system that would give the same resolution as conventional ground-based TEM soundings.

In 2006, as an alternative to a costly drilling campaign 0–300 m offshore, two test lines, each with a length of approximately 2000 m and 500 m apart, were flown for the county of Ribe starting 1000 m inland and ending 1000 m offshore. The purpose of the survey was to track the pollution plume related to the pits and to demonstrate the SkyTEM system's ability to measure the depth of the seawater in areas with shallow seawater. The two lines revealed the pollution plume from the pits and also indicated the freshwater plume extending under the seawater close to the shoreline as well as the saltwater intrusion moving inland (Christensen et al., 2009*b*).

In 2009, a more comprehensive survey was flown to investigate the pollution issues together with the distribution

of freshwater and saltwater in the area. After gaining permission to fly over military training grounds, the survey was conducted in one day, 24 April, in good weather conditions, recording both horizontal in-line ($x$) and vertical ($z$) component data in two interleaved moments: a super-low moment and a high moment. Auxiliary data included the GPS position, transmitter (Tx) altitude (measured using a laser altimeter) and Tx attitude (tilt of Tx frame in-line and perpendicular to flight direction). A total of 26 lines, each with a length of approximately 2500 m and 50 m apart were flown in a WNW–ESE direction, equally covering the offshore and onshore part of the area. The parameters of the survey are listed in Table 2 and in Figure 2 there is a location map where the survey lines are shown. Figure 3 shows the flight lines, the dumping pits and selected borehole locations.

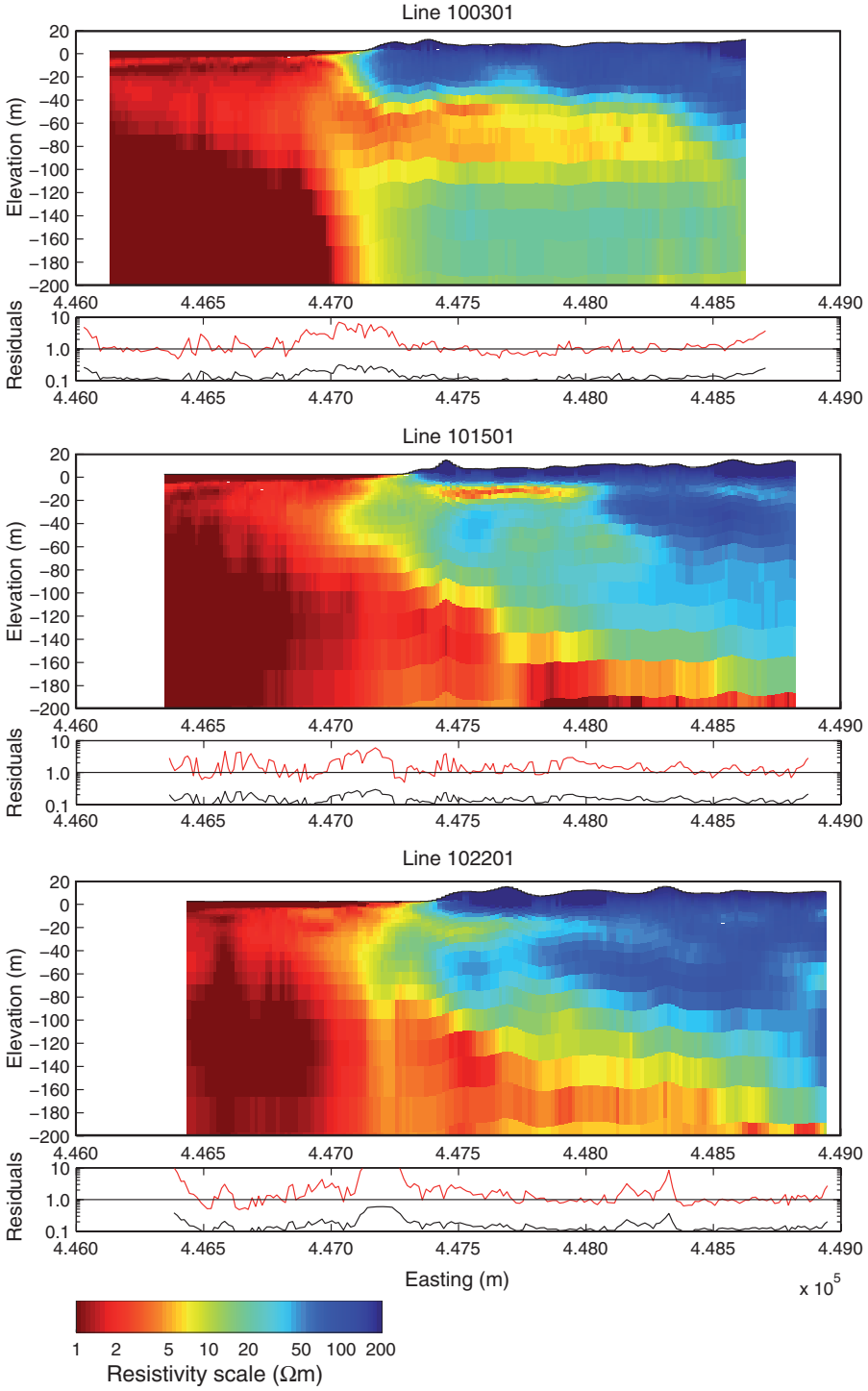


**Fig. 7.** Model sections of Lines 3, 15, 22 and 26 to a depth of 200 m. The data residual (red) and total residual (black) of the inversion is plotted below the model section. The elevation of the sea surface reflects the coordinate projection used (UTM WGS84 Z32) and the tidal situation on the day of data acquisition.

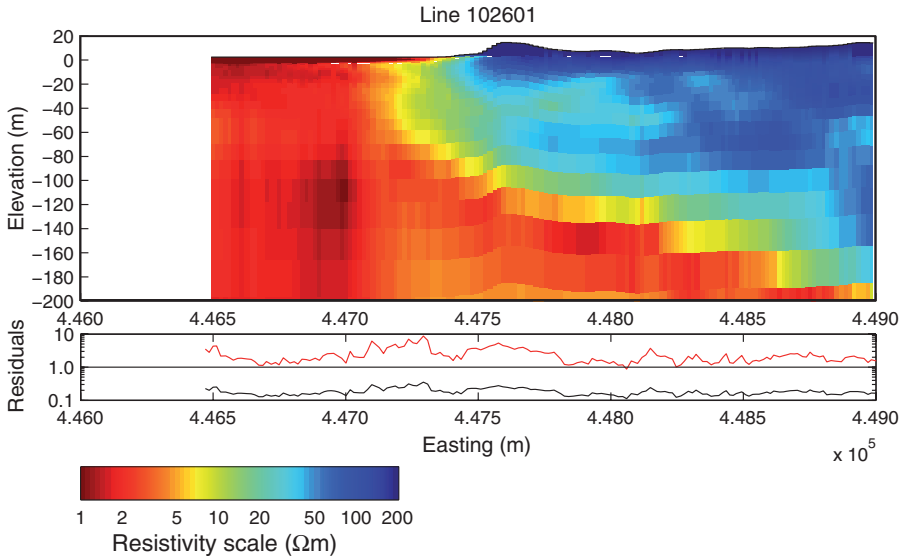


**Fig. 7.** (*continued*)

### *Data processing*

Signal strength was high in the area and the SkyTEM data were subjected to a basic data processing of simple stacking. Laser altimeter data were processed using a local maximum filter to attempt to recover distance to the ground surface. Data from each of the altimeters was then corrected for the attitude (tilt) of the Tx loop, and to yield the height above ground of the Tx loop centre. Final laser altitudes are averages of data from both altimeters. For a further discussion of these steps, please refer to Auken et al. (2009). In the data processing, no bias signal was found and repeated measurements demonstrated that there was no system drift.

### *Noise model*

Theoretically, the noise of TEM data collected with time gates with widths increasing linearly with time decreases with delay time, $t$, as $t^{-½}$ if the noise is white. For early times, the exponent may be between $-½$ and $-1$ due to the presence of monochromatic signals from AM transmitters. We use the general noise model

$$V_{noise} = V_0 \cdot \left(\frac{t\,[\mathrm{ms}]}{1\ \mathrm{ms}}\right)^{\alpha} \tag{4}$$

where $V_0$ is the noise level at 1 ms and $\alpha$ typically attains values between $-½$ and $-1$. Visually inspecting the data from the survey and adjusting $V_0$ and $\alpha$ gave a value of $V_0 = 3 \times 10^{-12}$ and $\alpha = -0.5$ for the super-low moment data and a value of $V_0 = 1 \times 10^{-13}$ and $\alpha = -0.5$ for the high moment data. The value of $V_0$ refers to data having been normalised with the Tx moment. A general relative noise floor of 0.03 was added to the absolute noise to account for dimensionality errors and other error sources not included in equation 3. $V$ being the signal strength, this gives a relative noise of

$$V_{noise}^{rel} = \sqrt{(V_{noise}/V)^2 + 0.03^2} \tag{5}$$

### *Inversion, data fit and data inconsistency*

The inversion was done using a fast inversion method based on an approximate expression for the apparent conductivity in the wavenumber domain, a development based on Christensen (2002) and Christensen et al. (2009*a*). The lateral correlation was implemented with a further development of the LPC method of Christensen and Tølbøll (2009) that ensures strictly horizontal constraints in multi-layer models.

One of the criteria for a successful inversion is that the residuals are appropriately small. The data residual, model residual and the total residuals are given by

$$R_d = \sqrt{\frac{1}{N}\left(d_{obs} - g(m_n)\right)^T C_{obs}^{-1}\left(d_{obs} - g(m_n)\right)} \tag{6}$$

$$R_m = \sqrt{\frac{1}{L}\left(\boldsymbol{m}_{prior} - \boldsymbol{m}_n\right)^T \boldsymbol{C}_m^{-1}\left(\boldsymbol{m}_{prior} - \boldsymbol{m}_n\right)} \tag{7}$$

$$R_t = \sqrt{\frac{1}{N+L}\left(N \cdot R_d^2 + L \cdot R_m^2\right)} \tag{8}$$

where $N$ and $L$ are the number of data and model layers, respectively.

In general, most of the soundings can be interpreted well with 1D models, although that in no way ensures that the conductivity structure is actually 1D (Ellis, 1998). Typical values of the normalised data residuals, equation 5, are of the order of 0.5–5 (see Figures 5 and 7), indicating that the noise model is reasonable. The total residual attains values of 0.1–0.3. However, at certain locations, primarily at the beach where the very well-conducting seawater meets the more resistive land formations, we see the inconsistency with the assumption of a 1D model expressed in a poorer data fit.

### *Presentation of results*

#### *Pollution from the dumping pits*

For the whole survey area, colour contoured maps of the mean resistivity in elevation intervals have been produced. The mean has been found over log(resistivity) in the elevation interval $[h_1;h_2]$ as

$$<\rho> = \exp\left[\frac{1}{h_2 - h_1}\int_{h_1}^{h_2} \log\left(\rho(z)\right) dz\right] \tag{9}$$

which, for a layered model with homogeneous layers, reduces to a simple sum. Plots of the mean resistivity in selected elevation intervals are shown in Figure 4.

Starting at the most shallow elevation interval in Figure 4 from −2 to 0 m, we see no sign of a lowered resistivity in the on-land part of the survey area. The first clear indication of a lowered resistivity is in the elevation interval −10 to −8 m, and it continues downwards to the elevation interval −18 to −16 m. We interpret this as being caused by the pollution from the dumping pits due to the presence of inorganic ions in the dumped fluids. The lower resistivity in the elevation interval −10 to −8 m shows inhomogeneities correlated with the most polluting pits, while the pollution plumes at deeper elevations coalesce into one plume for all pits. The signature is the strongest in the elevation interval −14 to −12 m; in the deeper parts the signature weakens. It is quite apparent that the area with the lowered resistivity is connected with the sea, confirming what has been found in boreholes at the coastline—that the pollution moves seawards. In the elevation intervals −30 to −28 m and −32 to −30 m, which is well below the silt layer in the area that is supposed to stop—or at least delay—the spreading of the pollution, we see a weak signature just below the major polluted area. The low resistivity area is repeated over several elevation intervals and we are confident that it signifies that part of the pollution plume has moved through the silt layer and that it furthermore seems to move not only seawards, but also southwards.

Due to the fact that the lithological information from the boreholes only covers the shallow subsurface and that there are very few deeper drillings in the area, it is in general quite difficult to distinguish between higher conductivities associated with the pollution (or the saltwater) and the higher conductivities of clays. However, for the area immediately below the pits, it is most likely that the lowered conductivity is caused by the pollution. First of all, the anomaly is conductive, meaning that it is well determined by the TEM method, and secondly, the silt layer which is present in the whole area does not seem to cause an increase in conductivity at the areas that are not close to the pits.

For each survey line, a model section of concatenated 1D models was produced and selected sections through the polluted area are shown in Figure 5.

The model sections confirm the extent of the polluted volume seen in the plot of mean resistivity in elevation intervals. The pollution plume starts to appear in Line 10 to then become stronger in Lines 12, 14 and 16. In the model sections of Lines 12 and 14, the deep part of the plume revealed in the elevation maps between elevations −30 and −40 m can be identified between Easting 447 500 m and 448 000 m.

### *The interface between freshwater and saltwater*

The plot frames of Figure 4 also reveal the distribution of saltwater/freshwater in the area. The deeper the elevation intervals, the further the saltwater/freshwater interface recedes seawards in the northern part of the survey area, while the saltwater/freshwater interface seems to retain its position at the shoreline in the southern parts of the area. At depths below the sea bottom, resistivities increase to 1–2 Ωm which is consistent with the seawater conductivity of 0.25 m (4 S/m) and the formation factors that can be expected in unconsolidated sediments.

To further illustrate the behaviour of the saltwater/freshwater interface at depth, Figure 6 shows the mean resistivity in elevation intervals from −44 to −120 m. In the southern part of the area, saltwater intrusion is evident down to an elevation of around −96 m, but going deeper it appears to recede seawards again and more freshwater starts to dominate.

In the northern part of the area, we continue to find freshwater under the sea within the unconsolidated sediments of the seafloor, but the deeper we look, the more the saltwater will start to move towards land and at an elevation of −88 to −96 m, it is again aligned with the shoreline. In the deeper parts, saltwater intrudes under land, and at an elevation of −120 m, it has moved more than 1 km inland. From an elevation of −100 m, the sediments under the sea appear to become more conductive. However, at these depths the posterior uncertainty of the model resistivities increases considerably; these formations lie below the depth of investigation that could be achieved with the SkyTEM system at the time of the survey. One must also remember that the lack of drilling information about the deeper lithology jeopardises the distinction between saltwater and clays.

To support the findings in the maps of mean resistivity in elevation intervals outlined above, Figure 7 displays the model sections of Lines 3, 15, 22 and 26 to an elevation of −200 m.

In the above paragraphs, we have interpreted the changes in resistivity as changes in the saltwater concentration, but the lack of information about the deeper parts of the geology opens up the possibility of alternative views. In particular, in the southern part of the area, the fact that the low resistivity zone disappears at depth invites other explanations of the hydrodynamics of the saltwater/freshwater interface: the distribution of saltwater and freshwater could be influenced by the presence of clayey formations controlling the hydrodynamics of the situation.

## Conclusions

We have presented a helicopterborne TEM survey from a coastal region at the North Sea in western Jutland, Denmark, carried out with the purpose of mapping the extent of a pollution plume and the coastal hydrogeology.

22 out of the 26 lines of the airborne electromagnetic data set with a spacing of 50 m were inverted with multi-layer models including vertical constraints through a model broadband covariance matrix. The remaining four lines were discarded due to coupling to pipelines. The inversion was laterally correlated in the plane using the LPC method.

The pollution plume is clearly indicated in the model sections and the maps of mean resistivity in elevation intervals and it was possible to delineate the extent of the plume from the survey results. The plume extends over an interval of 500 m NS and has its main strength in the elevation intervals from −10 to −20 m relative to sea level. The plume appears to move seawards as expected, but the inversion results also indicate possible seepage moving southward in the deeper parts of the polluted depth interval.

The interlacing of freshwater and saltwater forms a complex pattern mainly determined by differences in hydraulic conductivity of the permeable sediments and the presence of impermeable boundaries. Due to the lack of information from boreholes about the deeper geology, it is difficult to discern which structures are caused by differential hydraulic conductivity and which are determined by the presence of clays.

The airborne electromagnetic survey, though consisting only of a total of around 60 km and therefore being of limited cost, proved very useful in delineating the pollution plume and added new aspects to its hydrodynamics by indicating new seepage pathways. Furthermore, it delivered information on the complex structure of the saltwater/freshwater interface that should be included in any hydrogeological modelling.

## Acknowledgements

We are indebted to Jørgen Fjeldsted Christensen, Region South Jutland, for supplying the borehole information, informing us about the history of the pollution and giving us access to background material. For enlightening discussions along the way, we thank our colleagues Flemming Jørgensen, Holger Lykke-Andersen, Steen Christensen and Keld Rømer Rasmussen.

## References

Arbejdsgruppen vedrørende Kærgård Plantage, 2006, Forurening fra Esbjerg Kemi ved Kærgård Plantage: Delrapport nr. 6. In Danish (Pollution from Esbjerg Kemi at Kærgaard Plantage. Workgroup concerning Kærgaard Plantage: Report No 6).

Auken, E., and Christiansen, A. V., 2004, Layered and laterally constrained 2D inversion of resistivity data: *Geophysics*, **69**, 752–761.

Auken, E., Christiansen, A. V., Jacobsen, B.H., Foged, N., and Sørensen, K. I., 2005, Piecewise 1D laterally constrained inversion of resistivity data: *Geophysical Prospecting*, **53**, 497–506.

Auken, E., Pellerin, L., Christensen, N. B., and Sørensen, K., 2006, A survey of current trends in near-surface electrical and electromagnetic methods: *Geophysics*, **71**, G249–G260.

Auken, E., Christiansen, A. V., Westergaard, J. A., Kirkegaard, C., Foged, N., and Viezzoli, A., 2009, An integrated processing scheme for high-resolution airborne electromagnetic surveys, the SkyTEM system: *Exploration Geophysics*, **40**, 184–192.

Beamish, D., and Klinck, B., 2006, Hydrochemical characterization of a coal mine plume detected by an airborne geophysical survey: *Geofluids*, **6**, 82–92. doi:10.1111/j.1468-8123.2006.00130.x

Beuhler, M., 2003, Potential impacts of global warming on water resources in southern California: *Water Science and Technology*, **47**, 165–168.

Christensen, N. B., 2002, A generic 1-D imaging method for transient electromagnetic data: *Geophysics*, **67**, 438–447.

Christensen, N. B., 2009, Preface to the Special Issue on Airborne Geophysics: *Journal of Applied Geophysics*, **67**, 193–195. doi:10.1016/j.jappgeo.2009.03.001

Christensen, N. B., and Tølbøll, R. J., 2009, A lateral model parameter correlation procedure for one-dimensional inverse modelling: *Geophysical Prospecting*, **57**, 919–929. doi:10.1111/j.1365-2478.2008.00756.x

Christensen, N. B., Reid, J. E., and Halkjær, M., 2009*a*, Fast, laterally smooth inversion of airborne transient electromagnetic data: *Near Surface Geophysics*, **7**, 599–612. doi:10.3997/1873-0604.2009047

Christensen, N. B., Halkjær, M., and Sørensen, K. I. 2009*b*, Mineral and groundwater exploration with the SkyTEM system: 20th ASEG Geophysical Conference, Adelaide, Extended Abstracts, 1–5. doi:10.1071/ASEG2009ab134

Ellis, R. G., 1998, Inversion of airborne electromagnetic data: *Exploration Geophysics*, **29**, 121–127.

Faneca Sànchez, M., Gunnink, J. L., van Baaren, E. S., Oude Essink, G. H. P., Siemon, B., Auken, E., Elderhorst, W., and de Louw, P. G. B., 2012, Modelling climate change effects on a Dutch coastal groundwater system using airborne electromagnetic measurements: *Hydrology and Earth System Sciences*, **16**, 4499–4516. doi:10.5194/hess-16-4499-2012

Fitterman, D. V., and Stewart, M. T., 1986, Transient electromagnetic sounding for groundwater: *Geophysics*, **51**, 995–1005.

Fitterman, D. V., and Deszcz-Pan, M., 1998, Helicopter EM mapping of saltwater intrusion in Everglades National Park, Florida: *Exploration Geophysics*, **29**, 240–243.

Fitterman, D. V., Deszcz-Pan, M., and Stoddard, C. E., 1999, Results of time-domain electromagnetic soundings in Everglades National Park, Florida: U.S. Geological Survey Open-File Report 99-426, 1999, available on CD-ROM.

Goldman, M., Tabarovsky, L., and Rabinovich, M., 1994, On the influence of 3-D structures in the interpretation of transient electromagnetic sounding data: *Geophysics*, **59**, 889–901.

Günther, T., and Müller-Petke, M., 2012, Hydraulic properties at the North Sea island of Borkum derived from joint inversion of magnetic resonance and electrical resistivity soundings: *Hydrology and Earth System Sciences*, **16**, 3279–3291.

Gyulai, Á., and Ormos, T., 1999, A new procedure for the interpretation of VES data: 1.5-D simultaneous inversion method: *Journal of Applied Geophysics*, **64**, 1–17.

Hördt, A., and Scholl, C., 2004, The effect of local distortions on time-domain electromagnetic measurements: *Geophysics*, **68**, 87–96.

Hammack, R. W., Kaminskiy, V., Warner, K., and Kleinmann, R. L., 2005, Using helicopter electromagnetic surveys to identify potential hazards at coal waste impoundments: Proceedings of the 9th International Mine Water Congress, 125–132.

Inman, J. R. Jr., Ryu, J., and Ward, S. H., 1975, Resistivity inversion: *Geophysics*, **38**, 1088–1108.

Kirkegaard, C., Auken, E., Sonnenborg, T. O., and Jørgensen, F., 2011, Salinity distribution in heterogeneous coastal aquifers mapped by airborne electromagnetics: *Vadose Zone Journal*, **10**, 125–135. doi:10.2136/vzj2010.0038

Langevin, C. D., 2003, Simulation of submarine groundwater discharge to a marine estuary: Biscayne Bay, Florida: *Ground Water*, **41**, 758–771.

Menke, W., 1989, *Geophysical data analysis: discrete inverse theory*: Academic Press Inc.

Miljøstyrelsen og Ribe Amt, 2005, Redegørelse vedrørende Forureningen i Kærgård Plantage. Report in Danish (Assessment of the pollution at Kærgaard Plantation). Published by: Arbejdsgruppen vedrørende Kærgård Plantage (The Kærgaard Plantation Working Group). ISBN: 87-7941-682-9.

Morris, B., Shang, J., Howarth, P., and Witherly, K., 2002, Application of remote sensing and airborne geophysics to mine tailings monitoring, Copper Cliff, Ontario: 15th Symposium on the Application of Geophysics to Environmental and Engineering Problems, Expanded Abstracts, 1–14.

Newman, G. A., Anderson, W. L., and Hohmann, G. W., 1987, Interpretation of transient electromagnetic soundings over three-dimensional structures for the central-loop configuration: *Geophysical Journal of the Royal Astronomical Society*, **89**, 889–914.

Reid, J., Christensen, N. B., and Godber, K., 2012, SkyTEM helicopter transient electromagnetic surveys of tailings dams: 22nd ASEG Geophysical Conference, Extended Abstracts, 1–4. doi:10.1071/ASEG2012ab276

Ribe Amtskommune, Miljøministeriet, Danmarks Geologiske undersøgelse, Skov- og Naturstyrelsen, 1989, Redegørelse om muligheden for indvinding af ral og sand i Vejers-området. In Danish (Report concerning the possibility of sand and gravel extraction in the Vejers-area. Ribe County, Ministry of Environment, Danish Geological Survey, and Forest and Nature Agency).

Rutley, A., and Fallon, G., 2000, Electromagnetic surveys for environmental applications at mining operations – an Argentinean and Australian perspective: 70th SEG Annual Meeting, Expanded Abstracts, 19, 1239–1242.

Serban, D. Z., and Jacobsen, B. H., 2001, The use of broadband prior covariance for inverse palaeoclimate estimation: *Geophysical Journal International*, **147**, 29–40.

Shtivelman, V., and Goldman, M., 2000, Integration of shallow reflection seismics and time domain electromagnetics for detailed study of the coastal aquifer in the Nitzanim area of Israel: *Journal of Applied Geophysics*, **44**, 197–215.

Siemon, B., Steuer, A., Meyer, U., and Rehli, H.-J., 2007, HELP ACEH - A post-tsunami helicopter-borne groundwater project along the coast of Aceh, northern Sumatra: *Near Surface Geophysics*, **5**, 231–240.

Silvestri, S.,Viezzoli, A., Edsen, A., Auken, E., and Giada, M., 2009, The use of remote and proximal sensing for the identification of contaminated landfill sites: Proceedings of the 12th International Waste Management and Landfill Symposium (Sardinia Symposium), 5–9 October 2009.

Sørensen, K. I., and Auken, E., 2004, SkyTEM - A new high-resolution helicopter transient electromagnetic system: *Exploration Geophysics*, **35**, 191–199.

Steuer, A., Siemon, B., and Auken, E., 2009, A comparison of helicopter-borne electromagnetics in frequency- and time-domain at the Cuxhaven valley in Northern Germany: *Journal of Applied Geophysics*, **67**, 194–205. doi:10.1016/j.jappgeo.2007.07.001

Sulzbacher, H., Wiederhold, H.,Grinat, M., Igel, J.,Burschil, T., Günther, T., Siemon, B., and Hinsby, K., 2011, Calibration of density driven flow model for the freshwater lens beneath the North Sea Island Borkum by

geophysical data: Proceedings of the European Meeting of Environmental and Engineering Geophysics, 12–14 September 2011, Leicester, UK, P02.

Sulzbacher, H., Wiederhold, H., Siemon, B., Grinat, M., Igel, J., Burschil, T., Günther, T., and Hinsby, K., 2012, Numerical modelling of climate change impacts on freshwater lenses on the North Sea Island of Borkum using hydrological and geophysical methods: *Hydrology and Earth System Sciences*, **16**, 3621–3643. doi:10.5194/hess-16-3621-2012

Teatini, P., Tosi, L., Viezzoli, A., Baradello, L., Zecchin, M., and Silvestri, S., 2011, Understanding the hydrogeology of the Venice Lagoon subsurface with airborne electromagnetics: *Journal of Hydrogeology*, **411**, 342–354.

United Nations, 2004, A more secure world: our shared responsibility. Report of the High-level Panel on Threats, Challenges and Change.

United Nations, 2006, Beyond scarcity: power, poverty and the global water crisis. Human Development Report 2006. Published for the United Nations Development Programme (UNDP).

Viezzoli, A., Tosi, L., Teatini, P., and Silvestri, S., 2010, Surface water–groundwater exchange in transitional coastal environments by airborne electromagnetics: the Venice Lagoon example: *Geophysical Research Letters*, **37**, doi:10.1029/2009gl041572

Wiederhold, H., Sulzbacher, H., Grinat, M., Günther, T., Igel, J., Burschil, T., and Siemon, B., 2013, Hydrogeophysical characterization of freshwater/saltwater systems – case study: Borkum Island, Germany: *First Break*, **31**, 109–117.